

Performance of the *Far Ultraviolet Spectroscopic Explorer* mirror assemblies

Raymond G. Ohl^{*a}, Robert H. Barkhouser^b, Steven J. Conard^b, Scott D. Friedman^c, Jeffery Hampton^d,
H. Warren Moos^c, Paul Nikulla^d, Cristina M. Oliveira^c, Timo T. Saha^a

^aNASA/Goddard Space Flight Center, Greenbelt, Md.

^bInstrument Development Group, Johns Hopkins University, Baltimore, Md.

^cCenter for Astrophysical Sciences, Department of Physics and Astronomy,
Johns Hopkins University, Baltimore, Md.

^dSwales Aerospace, Inc., 5018 Herzel Place, Beltsville, Md.

ABSTRACT

The *Far Ultraviolet Spectroscopic Explorer* is a NASA astrophysics satellite which produces high-resolution spectra in the far-ultraviolet (90.5—118.7 nm bandpass) using a high effective area and low background detectors. The observatory was launched on its three-year mission from Cape Canaveral Air Station on 24 June 1999. The instrument contains four co-aligned, normal incidence, off-axis parabolic mirrors which illuminate separate Rowland circle spectrograph channels equipped with holographically ruled diffraction gratings and delay line microchannel plate detectors. The telescope mirrors have a 352 × 387 mm aperture and 2245 mm focal length and are attached to actuator assemblies, which provide on-orbit, tip, tilt, and focus control. Two mirrors are coated with silicon carbide (SiC) and two are coated with lithium fluoride over aluminum (Al:LiF). We describe mirror assembly in-flight optical and mechanical performance.

On-orbit measurements of the far-ultraviolet point spread function associated with each mirror are compared to expectations based on pre-flight laboratory measurements and modeling using the Optical Surface Analysis Code and surface metrology data. On-orbit imaging data indicate that the mirrors meet their instrument-level requirement of 50% and 95% slit transmission for the high- and mid-resolution spectrograph entrance slits, respectively. The degradation of mirror reflectivity during satellite integration and test is also discussed. The FUV reflectivity of the SiC- and Al:LiF-coated mirrors decreased about 6% and 3%, respectively, between coating and launch.

Each mirror is equipped with three actuators, which consist of a stepper motor driving a ball screw via a two-stage planetary gear train. We also discuss the mechanical performance of the mirror assemblies, including actuator performance and thermal effects.

Keywords: *FUSE*, satellites, ultraviolet, imaging, mirrors, reflectivity, actuators, optical systems, optomechanical design

1. INTRODUCTION

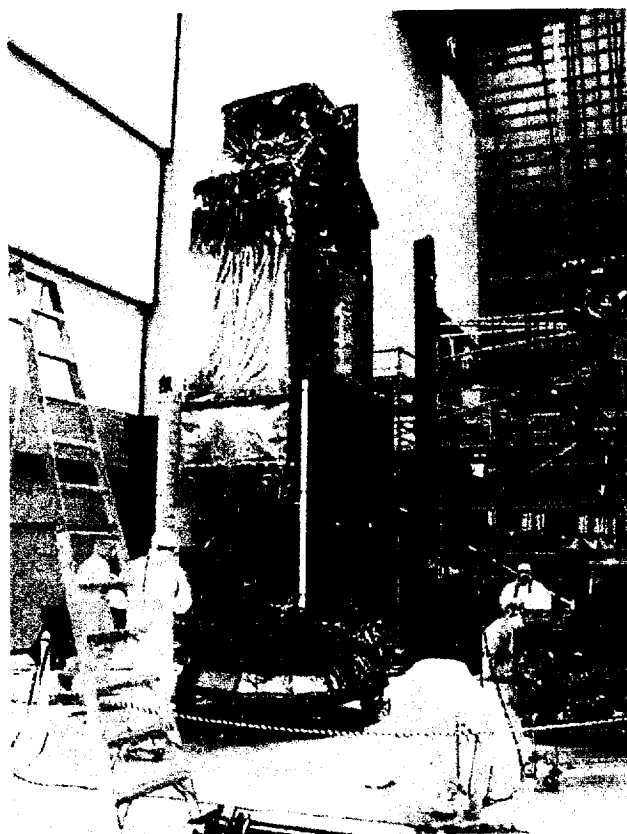
The *Far Ultraviolet Spectroscopic Explorer* (*FUSE*) is a NASA astronomy mission managed and operated by the Center for Astrophysical Sciences at the Johns Hopkins University (JHU)¹. *FUSE* was built by an international team of government, university, and corporate partners lead by JHU. The *FUSE* instrument examines the far-ultraviolet (90.5—118.7 nm; FUV) universe at high resolution ($\lambda/\Delta\lambda = 20,000$ —25,000) with a high effective area ($> 20 \text{ cm}^2$) using low background, large format detectors². A Boeing Delta II 7320-10 rocket placed *FUSE* in a 768 km, 25° inclination, near-circular orbit on 24 June 1999 for a three-year mission.

* Correspondence: Email: Raymond.G.Ohl@gsfc.nasa.gov; Telephone: 301-286-8368; Fax: 301-286-0204

The *FUSE* satellite consists of a science instrument and a spacecraft, which handles all support functions (Figure 1a). The instrument contains four co-aligned, normal incidence, off-axis parabolic telescope mirrors³, each of which illuminates a separate spherical, holographically ruled diffraction grating in a Rowland circle configuration (Figure 1b)⁴. In order to optimize instrument efficiency, the optics have different coatings: Two of the instrument channels use optics coated with silicon carbide (SiC) and two use lithium fluoride over aluminum (Al:LiF). One SiC- and one Al:LiF-coated channel form a pair covering the whole *FUSE* bandpass and their associated gratings are on essentially the same Rowland circle. Each pair of channels also shares one of two large-format, delay line microchannel plate detectors⁵. The spectrum from each channel falls in a different location on the two-dimensional detector. The parabolic telescope mirrors and Rowland circle spectrograph design maximize instrument efficiency by employing only two reflections prior to photon detection.

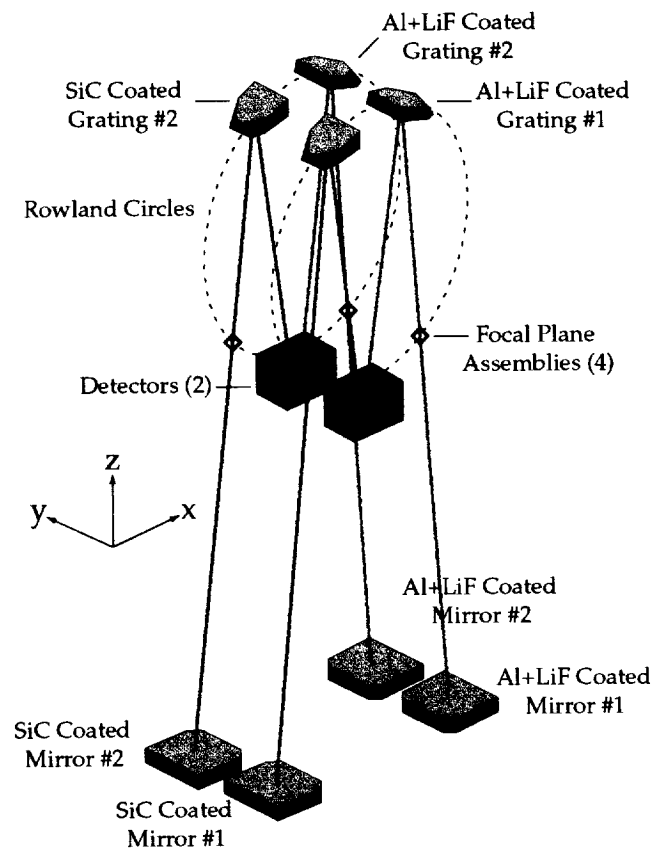
Each mirror is equipped with three actuators⁶, which consist of a stepper motor driving a ball screw via a two-stage planetary gear train. The actuators allow mirror motion in focus, tip, and tilt during flight.

After a discussion of the design of the telescope mirror assemblies (Section 2), we compare pre-launch predictions of imaging performance with on-orbit data (Section 3). We discuss mirror FUV reflectivity as measured prior to launch (Section 4). We also cover mirror actuator mechanical performance (Section 5). We conclude with a summary of the in-flight performance of the *FUSE* mirror assemblies (Section 6).



NASA

(a)



(b)

Figure 1. (a) Photograph of the *FUSE* satellite at NASA/Goddard Space Flight Center during integration. The larger, upper rectangular structure is the science instrument. The smaller structure below the instrument is the support spacecraft. The satellite is about 5.5 m high and 1300 kg total mass. (b) Schematic showing the *FUSE* optical components. The fine error sensor cameras are not shown. Note the orientation of the instrument coordinate system (after [1]).

2. OPTICAL AND MECHANICAL DESIGN

The *FUSE* instrument consists of two major subsystems: the telescope and spectrograph. The telescope is made up of four normal incidence, off-axis parabolic mirrors which are co-aligned and co-pointed (target acquisition is accomplished using satellite pointing). The mirrors have a 352×387 mm aperture and 2245 mm focal length (Figure 2a)³. The sections do not contain the vertex of the parent paraboloid --- the vertex is about 34.5 mm from the edge of the mirror aperture in x (see Figure 1b for coordinate definitions). The off-axis angle is about 5.5° , but this value differs slightly for the SiC- and Al:LiF-coated mirrors as required for different grating incidence angles and is set by the location of an aperture stop in front of the mirrors. Except for the optical surface coating, the mirror assemblies are thus identical. The optical axes of each mirror are well separated on the optical bench, forming four independent telescope channels.

Each mirror substrate is made of Zerodur and is ~70% weight-relieved for a final mass of 7.7 kg in an open-back, triangular isogrid pattern (Figure 2b).[†] The minimum facesheet thickness is 7.5 mm. Three blade flexures, oriented with soft axes radial to the center of the mirror, connect the mirror with an intermediate plate (Figure 2c and e). The intermediate plate is attached to the actuator assembly (Figure 2d) via six post flexures (Figure 2e): Three axial post flexures, which support the upper assembly in z, are co-axial with the actuator ball screws and connect them to the composite intermediate plate. Three additional, lateral post flexures secure the upper assembly for translation in the x-y plane (perpendicular to the optical axis). The intermediate plate isolates the mirror from moments that can be induced by adjustments of the mirror actuators. A rectangular "pie pan" rigidly attaches to the intermediate plate, enclosing the mirror on five sides. An Al aperture stop is fixed to the top rim of the pie pan (Figure 2f).

The performance of this semi-kinematic mount during assembly and component-level mirror testing has been presented elsewhere⁷. The epoxy applied to the blade flexure-mirror rib bondline (Figure 2c) shrank upon cure, stressing the mirror substrate and increasing figure error. Further distortion associated with attaching the intermediate plate resulted in the figure error shown in Figure 3a.

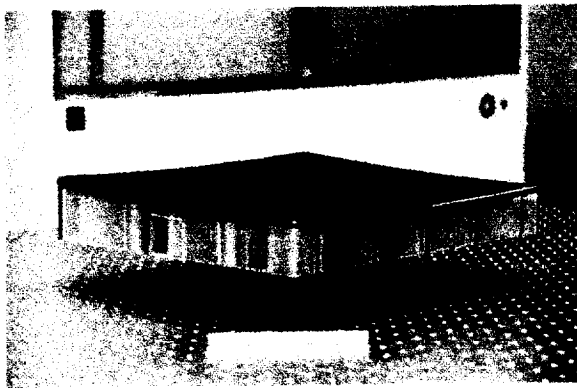
The telescope mirrors are attached to actuator assemblies⁶, which provide on-orbit tip, tilt, and focus control (Figure 2d). There are three actuators per mirror assembly. They provide the mirror with a focus resolution of $0.350 \mu\text{m}$ over a ± 2.1 mm range and a tip/tilt resolution of 0.160 arcsec over a ± 32.34 arcsec range. The actuator mechanism consists of a 30° , 3 phase, brushless stepper motor with an integral 160:1 two stage planetary gear reduction system (Figure 4). The motor/gearhead output pinion rotates a large spur gear providing an additional reduction of 4.25:1. The large spur gear has an integral lower housing section that supports a ball screw assembly. The housing is coupled to a pair of ball screw nuts, which provide a zero backlash translation of 2.540 mm per revolution. With a total gear reduction of 681:1 and a ball screw lead of 2.540 mm, an output translation of $0.310 \mu\text{m}$ per 30° motor step of rotation results. To signal the actuator's position at the middle and each end of travel (± 1.2 mm) a light emitting diode and encoder disk assembly (coupled to the gear housing) is used. At ± 1.2 mm of travel (the operating stroke), the position sensor is enabled and the motor step commands are disabled. In the event the electronic stop malfunctions, a non-jamming hard stop is encountered at ± 2.1 mm, which will stall the motor without inducing any damage to the actuator components.

Each assembly has a bed of strip heaters on the side of the intermediate plate closest to the mirror (Figure 2e). The heaters hold the assembly to $22^\circ \pm 5^\circ$ C.

A separate focal plane assembly (FPA) exists at the focus of each mirror⁸. Each FPA has three entrance slits for its associated spectrograph channel: a high-resolution slit (HIRS) which is 1.25×20 arcsec; a mid-resolution slit (MDRS) which is 4×20 arcsec; and a low-resolution slit (LWRS) which is 30×30 arcsec. The HIRS is on the mirror optical axis. The MDRS and LWRS are positioned about 100 arcsec off-axis on either side of the HIRS in y, parallel to the long axis of the slit. A source is placed in one of the slits using satellite pointing, but each FPA can translate independently in x and z for channel coalignment and focus.

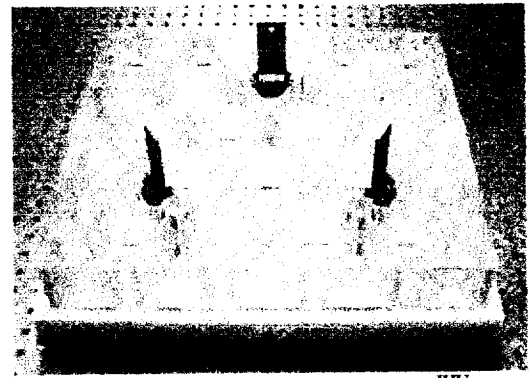
The FPA surface facing the mirror is coated with Al. A separate slit-jaw camera images the sky on this surface for each LiF channel. These fine error sensor (FES) cameras function in the visible with a complement of filters and are used for target acquisition and fine guidance⁹.

[†] Silicon Valley Group, Inc., Tinsley Division, Tinsley Laboratories, 3900 Lakeside Drive, Richmond, Ca. fabricated the mirrors and attached the blade flexures to the substrate.



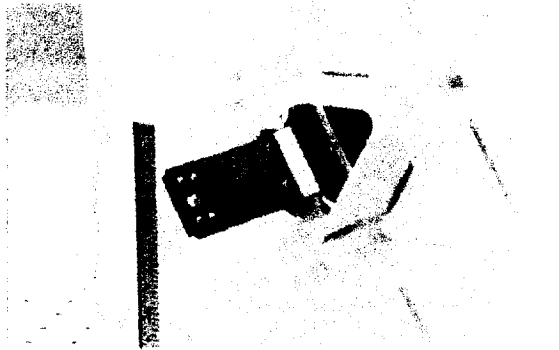
JHU

(a)



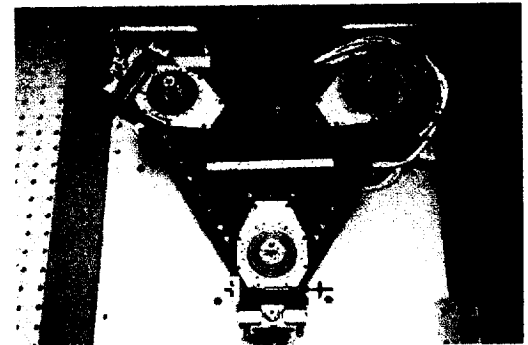
JHU

(b)



JHU

(c)



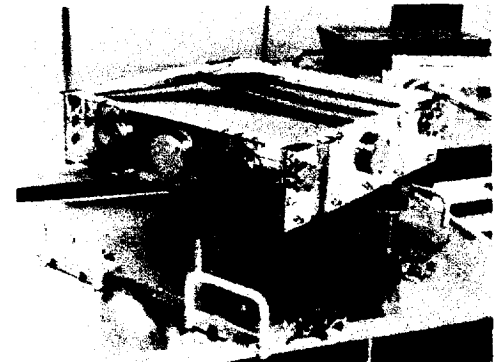
Swales Aerospace, Inc.

(d)



Swales Aerospace, Inc.

(e)



JHU Applied Physics Laboratory

(f)

Figure 2. (a) FUSE mirror resting face up on its flexures. (b) FUSE mirror face down showing lightweighting. (c) Close-up of mirror flexure showing Ti blade flexure pinned to Invar fitting, which is bonded to the Zerodur rib. (d) Face-on view of mirror actuator assembly showing the three actuators and composite structure. (e) Mirror assembly showing aluminum dummy "mirror," composite intermediate plate, and actuator assembly mounted to a handling fixture. (f) Full flight mirror assembly (with "pie pan" thermal enclosure and aperture stop installed) mounted to a handling fixture.

3. IMAGING PERFORMANCE

The component-level imaging specification for the telescope mirrors is given in terms of encircled energy: The mirrors must focus 90% of the energy at $\lambda = 100$ nm within a circle 1.5 arcsec ($16 \mu\text{m}$) in diameter. This specification is driven by the slit transmission requirement for the HIRS and instrument spectral resolution for the wider slits. Laboratory imaging measurements, surface metrology, and analysis using the Optical Surface Analysis Code (OSAC) at NASA/Goddard Space Flight Center (GSFC) confirmed that the mirrors met the requirement^{10,11}. The OSAC code was developed for other short wavelength, space astronomy missions to predict imaging performance based on metrology data. OSAC uses optical

prescription and figure error input to calculate spot broadening from geometric effects using a raytrace code. Additional image broadening from aperture diffraction and scattering off of small-scale mirror surface errors (mid-frequency errors and microroughness) is modeled using scalar diffraction theory¹¹. This analysis was verified by laboratory image tests at UV wavelengths longer than the FUSE bandpass¹⁰. The OSAC-predicted FUV point spread function is shown in Figure 3b.

Telescope-level FUV imaging requirements are more generous, as they include other contributions to image broadening, such as aberrations associated with off-axis slits, satellite pointing errors, telescope coalignment stability, defocus, etc. The requirements were generated early in the project design phase via a modulation transfer function analysis and are given in terms of slit transmission across the *FUSE* bandpass: $\geq 50\%$ for the HIRS and $\geq 95\%$ for the MDRS¹².

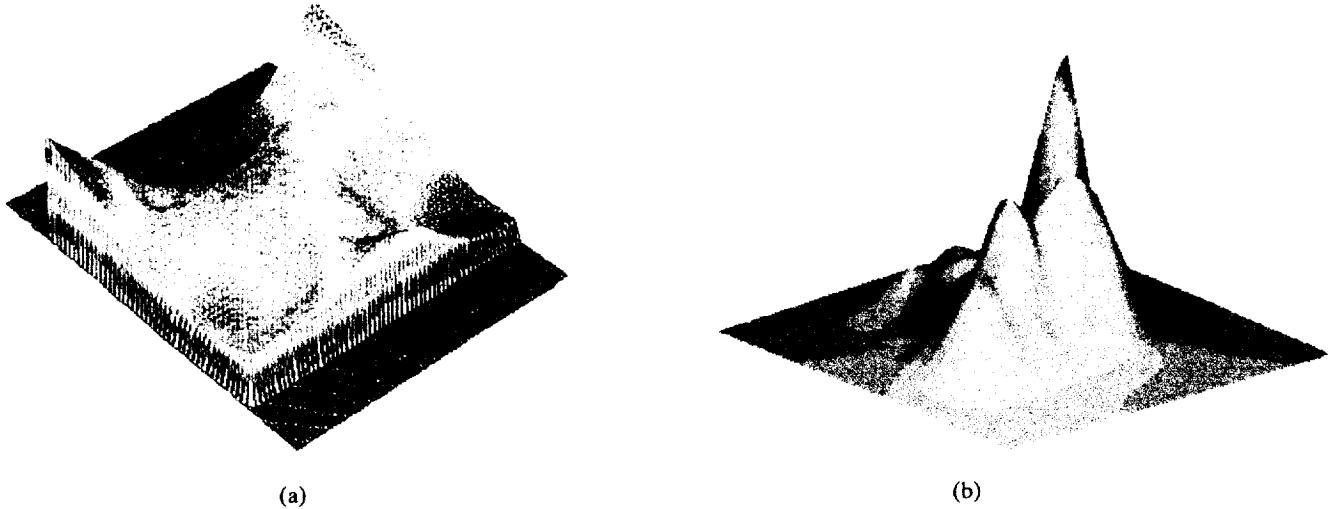


Figure 3. (a) Surface plot of figure error for the LiF 2 *FUSE* mirror after assembly and prior to integration with the instrument. The amplitude of the distortion is 0.046λ RMS at $\lambda = 632.8$ nm (after [7]). (b) Surface plot of predicted *FUSE* mirror point spread function at $\lambda = 100$ nm (after [10]). The low, broad shoulder arises from the asymmetric figure error shown in Figure 3a.

3.1. Mirror Focus

The distance from the mirror to the FPA, or “mirror focus,” was adjusted separately during flight for each of the four channels. The instrument was focused pre-flight, but the accuracy of this adjustment was limited by collimator performance¹³. Furthermore, gravity release and moisture desorption from the structure after launch altered the locations of the optical elements.

The best mirror focus is determined by means of a knife edge scan. The knife edge scan or distribution (KED) is the edge response, or

$$KED(x', z_0) = \int_0^{x'} \int_{-\infty}^{+\infty} \rho(x, y, z_0) dy dx, \quad (1)$$

where here x and y are Cartesian coordinates in the image plane, z is focus, ρ is the image, x' is distance in the direction normal to the knife edge, z_0 is the position of the knife edge in focus, and it has been assumed that the size of the knife edge is much larger than the size of the spot. An on-orbit KED is generated for a given telescope mirror by scanning an edge of the MDRS or LWRS across the image of a star and recording total FUV detector signal as a function of edge position.

The negative derivative of the KED is the line spread function (LSF) or line response,

$$LSF(x', z_0) = -\frac{dKED(x', z_0)}{dx'} = \int_{-\infty}^{+\infty} \rho(x', y, z_0) dy. \quad (2)$$

When the knife edge passes through the beam at best focus, the magnitude of the LSF is greatest and its width is smallest. Mirror focus adjustments were made by moving the FPAs in the z direction. The mirror focus was optimized using this method to $\approx 50 \mu\text{m}$. The absolute on-orbit focus adjustment was $< 100 \mu\text{m}$ for each channel, which is consistent with pre-flight predictions. The expected ground-to-orbit focus change associated with the metering structure alone was $< 50 \mu\text{m}$, but focus uncertainty from mirror installation on the optical bench increased the expected value to $< 100 \mu\text{m}$.

The FES has no independent focus mechanism. FES-A (LiF 1) has been used almost exclusively in flight. Changes in the positions of the LiF 1 mirror or FPA will change the focus of the FES. We found that star identification and tracking performance using FES-A was somewhat compromised at the best focus position for FUV performance in the LiF 1 channel⁸. Therefore, the LiF1 FPA was moved $\sim 100 \mu\text{m}$ in focus toward the mirror from its nominal position. This caused little degradation in performance for FUV observations using the LWRS and MDRS slits. For HIRS observations, a penalty in slit transmission is expected (Table 2), but this was deemed preferable to the increased risk of losing observations from failed acquisitions.

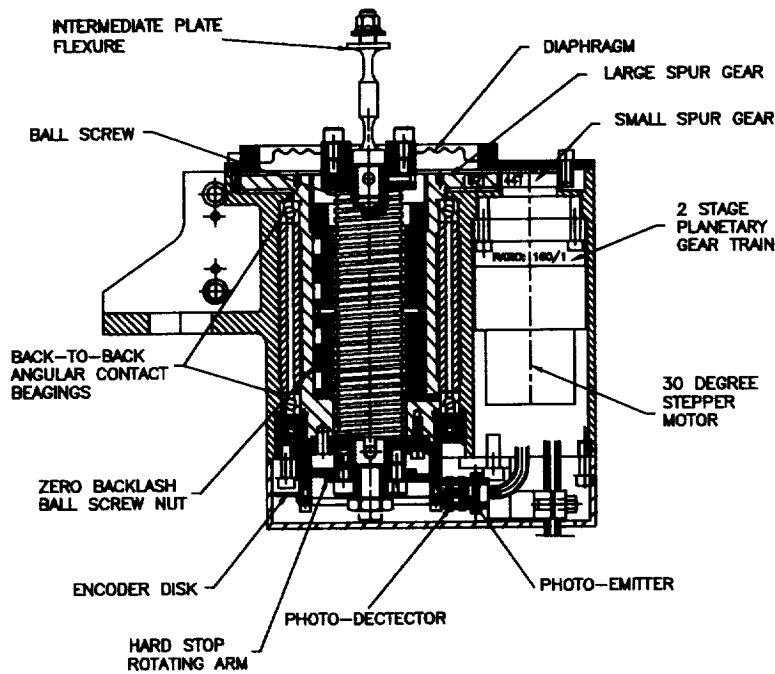


Figure 4. Drawing of the cross section of a mirror actuator mechanism (after [5]).

3.2. In-Flight Imaging Data

The OSAC-predicted slit transmissions at best focus and corresponding instrument-level requirements are listed in Table 1. Separate values are given for the SiC- and Al:LiF-coated mirrors, since they have different surface error. The somewhat greater surface roughness for the Al:LiF-coated mirrors is associated with schedule pressure during the fabrication phase, but all of the mirrors had surface error that met specification upon delivery to JHU^{7,10}. For this modeling, “best focus” is defined as the focus location for the image with the smallest RMS spot size.

As mentioned previously, the focus for the SiC 1, LiF 2, and SiC 2 mirrors was optimized to about $\pm 50 \mu\text{m}$ for FUV observations, while the focus for the LiF 1 mirror is off by $\sim 100 \mu\text{m}$ to support FES-A observations. The OSAC-predicted

slit transmissions including these values of defocus are listed in Table 2. The surface error characteristics for a SiC-coated mirror were used in this calculation, but the results would differ by < 3% for a LiF-coated mirror.

Mirror Pair	FWHM _{jitter} = 0.25 arcsec		FWHM _{jitter} = 0.5 arcsec	
	HIRS (%)	MDRS (%)	HIRS (%)	MDRS (%)
(requirement)	≥ 50	≥ 95	≥ 50	≥ 95
SiC-coated	92	98	89	98
Al:LiF-coated	88	93	85	93

Table 1. Modeled on-orbit slit transmission at $\lambda = 100$ nm for two different spacecraft pointing errors with no defocus and no off-axis aberrations (errors are $\pm 5\%$; after [10]). Instrument-level requirements are also given.¹²

On-orbit measurements of slit transmission are given in Table 3. These data are derived from the total signal from one ~9 nm section of the detector associated with a given mirror. These numbers thus represent the slit transmission for a significant portion of the *FUSE* bandpass, albeit weighted with the spectral energy distribution of the target star. For these data, the stars were the white dwarfs CPD-721184 and WD2211-495, which have relatively flat FUV spectra. For a source with a flat spectrum, the slit transmission is sensitive to wavelength only on the ~1% level¹¹. The target was placed in the slit and the total detector count read in “time-tagged” mode. Data were reduced only for those time intervals where the count rate was roughly constant (i.e., while mirror coalignment was thought to be accurate to less than the width of the slit, so the edge of the slit was supposedly not occulting the star). The data were not background subtracted, but the background signal is negligible compared to the count rate from these bright stars². 100% transmission is defined as the signal when observing the target through the LWRS.

Slit	LiF 1	Other Mirrors	
	100 μ m toward mirror	50 μ m toward mirror	50 μ m away from mirror
MDRS (%)	96	96	96
HIRS (%)	64	79	90

Table 2. Modeled on-orbit slit transmission at $\lambda = 100$ nm for FWHM_{jitter} = 0.35 arcsec and three different values for defocus (errors are $\pm 5\%$). The ~10% difference between the HIRS transmission at +50 μ m and -50 μ m from focus is due to the asymmetric energy distribution in the beam caused by the peculiar figure error on the mirrors (Figure 3a). The values for MDRS transmission include the aberrations associated with that slit’s 102.7 arcsec off-axis distance.

On average, the mirrors perform better than the instrument-level requirements for HIRS FUV transmission (an average of $65 \pm 2\%$ vs. the requirement of $\geq 50\%$), and marginally meet their specification for MDRS FUV transmission (an average of $93 \pm 2\%$ vs. the requirement of $\geq 95\%$). LiF 1 is not included in these averages, because, since LiF 1 has more effective area and on-target time than the other channels, there is a significant drop in gain for the region of the detector in the vicinity of the image of the LiF 1 LWRS, and the raw slit transmission measurements for LiF1 are not reliable. The values for LiF 1 in Table 3 are thus artificially high.

Within the uncertainty associated with the data and the prediction, all of the mirrors match the OSAC-prediction for on-orbit MDRS transmission, except SiC 1, which shows marginally less transmission than expected. This could be due to greater defocus for this channel, or possibly a change in the surface error for this mirror after integration. The first explanation is more likely, because the focus data are least complete for the SiC 1 channel. Motion of the image due to flexure of the instrument bench during the observation could also have decreased the transmission.

For LiF 1, the most defocused mirror, the measured on-orbit HIRS transmission agrees well with the prediction, within the quoted uncertainty. However, this is not surprising, given that defocus is large for this mirror and is a dominant factor in the spot size. For SiC 2, the on-orbit HIRS transmission is consistent with expectations for a FPA defocused $\sim 50 \mu\text{m}$ toward the mirror. For SiC 1 and LiF 2, the HIRS transmission is significantly worse than expected for the expected defocus. This could indicate up to a factor of 2 greater defocus than inferred from the on-orbit focus data, that significant flexure of the instrument bench occurred during the observation, and/or that the mirror figure error increased after integration.

On-orbit FUV KEDs generated using repeated passes of both edges of the MDRS are shown in Figure 5 for the LiF 1 and 2 mirrors, as well as OSAC-predicted KEDs for the relevant states of defocus. The knife edge step size is 1 arcsec. KED data do not exist for the SiC 1 and 2 mirrors. The scatter in the data for a given edge location is associated with repeated passes (consecutive sampling) across the focal plane with the MDRS. The noise is therefore indicative of systematic errors in the observation --- probably flexure in the instrument bench about the x and y axes on a timescale smaller than that associated with the execution of the KED.

The LiF 1 KED data are consistent with the prediction for a spot that is defocused by $100 \mu\text{m}$. However, in agreement with the aforementioned HIRS transmission data, the LiF 2 KED is consistent with an image that is broader than expected for only $\sim 50 \mu\text{m}$ of defocus. Unanticipated defocus, bench flexure on short timescales, and an increased mirror figure error after integration are all potential causes of this broadening. However, the relative smoothness of the LiF 1 KED vs. the more scattered LiF 2 data implicates bench flexure as a dominant factor in the spot size (since the LiF 1 mirror is used for satellite guidance using FES-A, the LiF 1 image is by definition stable with respect to the slit). Mirror rotations due to bench flexure with an amplitude of order 1 arcsec about the y axis and period ≤ 5 min would be sufficient to cause this broadening. Rotations of this amplitude and time scale were also observed when KEDs were generated during the focus program.

No reliable measurements of wide-angle, FUV scatter from the telescope mirrors have been made in-flight.

	LiF 1 (%)	SiC 1 (%)	LiF 2 (%)	SiC 2 (%)
MDRS / LWRS	104 ± 1	88 ± 3	96 ± 2	94 ± 6
HIRS / LWRS	57 ± 6	58 ± 3	60 ± 3	76 ± 2

Table 3. In-flight FUV slit transmission. The spacecraft pointing error is about 0.35 arcsec FWHM.⁹ The errors are the standard deviation of a set of multiple measurements. A drop in gain for regions of the detector in the vicinity of the image of the LWRS for LiF 1 causes the MDRS transmission for this mirror to appear to be greater than 100%.

4. MIRROR REFLECTIVITY

The FUV reflectivity of the Al:LiF coating decreases with exposure to moisture^{14,15}. Prior to launch, the Al:LiF-coated mirrors were never exposed to a relative humidity (R/H) greater than 50% at room temperature. We limited the total exposure to a non-purged environment with R/H < 50% to about 100 hours. In addition, the mirrors were exposed to a R/H \approx 10% environment for about 10 days.

Mirror reflectivity was monitored during satellite integration and test using a system of “witness coupons.” This was accomplished by fabricating several 25 mm diameter flat mirrors in parallel with each flight mirror (i.e., coating occurred simultaneously with each flight mirror). These small witness mirrors accompanied the flight mirrors through each phase of integration and test, experiencing the same contamination and thermal environments. Their FUV reflectivity was measured periodically using a FUV reflectometer¹⁶. Witness mirror reflectivity over time during integration and test is shown in Figure 6. Spare witness mirrors were also used to verify an environment in advance of flight hardware exposure.

The flight mirrors themselves underwent a FUV reflectivity test prior to integration with the instrument. The flight mirror reflectivity requirements were $\geq 32\%$ for the SiC-coated mirrors, $\geq 60\%$ for the Al:LiF-coated mirrors for $\lambda > 105 \text{ nm}$, and \geq

38% for the Al:LiF-coated mirrors for $\lambda = 100\text{--}105\text{ nm}$. The mirrors met specification, but the errors on the measurements were about $\pm 20\%$.

Al:LiF-coated witness mirror reflectivity at $\lambda = 106.7\text{ nm}$ was about $70 \pm 3\%$ after coating and decreased to about $67 \pm 3\%$ shortly before launch. The reflectivity of the SiC-coated witness mirrors at $\lambda = 121.6\text{ nm}$ was about $40 \pm 2\%$ after coating and decreased to about $34 \pm 2\%$ shortly before launch (Figure 6; see [14] and [15] for discussion of the decrease in reflectivity over time for these coatings).

Some on-orbit degradation in reflectivity is expected due to the accretion of contamination from the rest of the satellite and interaction with atomic oxygen. The latter would be expected primarily at ram crossing, but pointing near the ram direction is completely avoided in flight. Instrument effective area has decreased 5–10% over the last 7 months, but this is most likely attributable to a drop in detector gain. No independent measurement of mirror on-orbit reflectivity is possible.

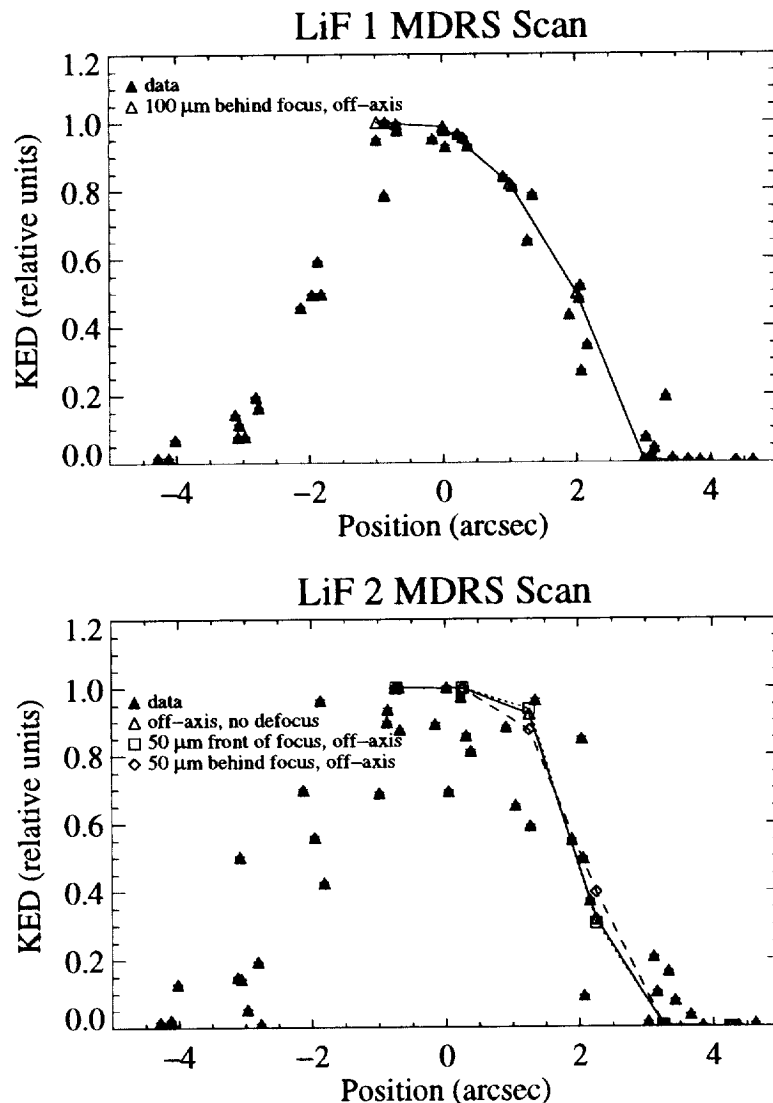


Figure 5. *FUSE* LiF 1 and LiF 2 flight mirror knife edge distributions (KED) obtained on-orbit using the MDRS (solid triangles). LiF 1 is defocused by $\sim 100\text{ }\mu\text{m}$. LiF 2 is defocused by $\sim 50\text{ }\mu\text{m}$ and also suffers from image motion during the knife edge scan. The error bars reflect photon statistics only. Also shown are modeled FUV KEDs as a function of focus generated using OSAC (open symbols). The model includes the aberrations associated with the MDRS' 102.7 arcsec off-axis distance.

5. MECHANICAL PERFORMANCE

5.1. Actuators

In flight, there have been no anomalies that can be attributed to the performance of the mirror actuator mechanisms.

As a cost savings step, the actuators were designed with no feedback system (e.g., an encoder). It was thought that the mirror actuators would be seldom used and that optical focus and alignment data would be sufficient for determining relative mirror position. In practice, the actuators are used more often than originally envisioned (with no impact to motor health) and motor position is tracked by counting motor steps on the ground using very tedious processes. Actuator use is somewhat complicated by the lack of encoder output, but this has no performance impact.

For focus motions, all three actuators are moved at once. For tip or tilt motions, the baseline procedure was to move opposing actuators in opposite directions, so that mirror focus would remain constant. However, once in-flight, the procedure was changed to move only one actuator in order to activate the mechanisms as little as possible, simplifying the procedure for satellite operations. The resulting defocus produces a negligible increase in image size.

Due to image motion caused by coupling of the instrument secondary structure to the optical bench, the number of mirror motions required is much higher than predicted before launch. The actuators were designed for far more motions than could reasonably be done in even a very long extended mission, so there is no cause for concern. Additionally, loss of a single actuator on any number of mirrors is a soft failure that will cause minimal loss of data.

Actuator range of motion was a product of the instrument optical error budget and the methods envisioned for on-orbit focus and alignment. In practice, less than 20% of the actuators' range of motion is used. The mirror actuators have not run over their entire range of motion in flight, as the risk of doing so is not justified. The largest excursions performed to-date have been driven by the focusing tests --- typically about one quarter of the full range. The mirror actuators are all within the center 25% of their total range of motion as limited by a soft stop. There is no indication that range of motion of the mirror actuators will be a limiting factor in the life of the mission.

There has been no explicit test of the accuracy of the mirror motions. Peak-up test data show motion accuracies for rotations about the y-axis for the SiC 1, LiF 2, and SiC 2 mirrors of < 2 arcsec for small (< 6 arcsec) motions. Moderate size motions (< 30 arcsec) have accuracies of < 4 arcsec. However, these measurements reflect less on the true accuracy of the actuators and more on the limitations in attempting to measure the inaccuracies. No statement can be made with respect to trending.

5.2. Thermal Effects

Image motion parallel to the y-axis and 1—2 arcsec in amplitude has been observed for LiF 2 and SiC 2 that matches the cycling of heaters on the instrument optical bench beneath the mirror intermediate plate. The typical cycling period for these heaters is about 300 sec. Since this motion is parallel to the long axis of the slit, this problem does not impact the science data.

6. CONCLUSION

From the standpoint of optical testing and modeling, our program has shown that a combination of reliable metrology, limited laboratory image testing, and analysis that has significant heritage can be a viable alternative to extensive, in-band image testing in the FUV. However, on-orbit measurements of imaging performance are too unreliable to make a definitive judgment at this time as to the final accuracy of this effort --- nevertheless, the data presented here are consistent with pre-flight predictions. Lack of coalignment stability is a problem with the optical bench, not the mirror assemblies. In spite of the stability problems, the mirrors meet the telescope-level requirements for FUV HIRS and MDRS transmission.

The small decrease in the FUV reflectivity of the mirrors during integration and test is a major success of the *FUSE* optics program. The witness mirror system benefited greatly from heritage from the *Hopkins Ultraviolet Telescope* program, which was part of the *Astro* Space Shuttle missions.

Although their duty cycle is much greater than anticipated pre-flight, the mirror actuator mechanisms have presented no problems and have performed to specification within the accuracy of our measurements.

Instrument spectral resolution when using the HIRS is about 10% greater than when using the LWRS. This value is greater than pre-flight expectations, because the effective telescope point spread function over an integration is larger than expected. We attribute this to defocus and co-alignment instability.

ACKNOWLEDGEMENTS

We are indebted to the hard work and dedication of the many people who contributed to the *FUSE* mirror program. Specifically, we gratefully acknowledge the *FUSE* spacecraft operations and mission planning team at JHU. *FUSE* is supported through the Explorers Program office at NASA/Goddard Space Flight Center and NASA contract NAS5-32985.

REFERENCES

1. H. W. Moos et al. "Overview of the *Far Ultraviolet Spectroscopic Explorer* Mission," *Astrophysical Journal* **538**, pp. L1—L6, 2000.
2. D. J. Sahnou et al. "On-Orbit Performance of the *Far Ultraviolet Spectroscopic Explorer* Satellite," *Astrophysical Journal* **538**, pp. L7—L12, 2000.
3. M. J. Kennedy, S. D. Friedman, R. H. Barkhouser, J. Hampton, and P. Nikulla. "Design of the *Far Ultraviolet Spectroscopic Explorer* mirror assemblies," *Proc. SPIE* **2807**, pp. 172—183, 1996.
4. E. Wilkinson, J. C. Green, S. N. Osterman, K. R. Brownsberger, and D. J. Sahnou. "Integration, Alignment, and Initial Performance Results of the *Far Ultraviolet Spectroscopic Explorer* (FUSE) Spectrograph," *Proc SPIE* **3356**, pp. 18—29, 1998.
5. O. H. W. Siegmund, M. Gummin, G. Gaines, G. Naletto, J. Stock, R. Raffanti, J. Hull, R. Abiad, T. Rodriguez-Bell, T. Magoncelli, P. Jelinsky, W. Donakowski, and K. Kromer. "Performance of the double delay line microchannel plate detectors for the *Far Ultraviolet Spectroscopic Explorer*," *Proc. SPIE* **3114**, pp. 283—294, 1997.
6. P. Nikulla. "The FUSE Mirror Mechanism," *Proc. 31st Aerospace Mechanism Symposium*, NASA CP-3350, 1997.
7. R. G. Ohl, R. H. Barkhouser, M. J. Kennedy, and S. D. Friedman. "Assembly and test-induced distortions of the FUSE mirrors --- lessons learned," *Proc. SPIE* **3356**, pp. 854—865, 1998.
8. K. Brownsberger, J. P. Andrews, G. Allison, and J. C. Westfall. "Performance of the FUSE focal plane assemblies," *Proc. SPIE* **4139**, 2000, this volume.
9. J. W. Kruk, P. Chayer, J. B. Hutchings, C. L. Morbey, and R. G. Murowski. "Fine Error Sensor optical performance," *Proc. SPIE* **4139**, 2000, this volume.
10. R. G. Ohl, T. T. Saha, S. D. Friedman, R. H. Barkhouser, and H. W. Moos. "Imaging performance of telescope mirrors for far-ultraviolet astronomy," *Appl. Opt.*, 2000, in press.
11. T. T. Saha, R. G. Ohl, S. D. Friedman, and H. W. Moos. "Optical Performance Modeling of FUSE Telescope Mirror," *Computational Optics and Imaging for Space Applications*, conference held at NASA/Goddard Space Flight Center, 2000, in press.
12. *FUSE* Instrument and Science Operations Team. *FUSE Instrument Requirements Document*, FUSE-JHU-0004, Revision B, Johns Hopkins University, Baltimore, 1996.
13. S. J. Conard, K. W. Redman, R. H. Barkhouser, D. B. McGuffey, S. Smee, R. G. Ohl, and G. D. Kushner. "Hardware and methods of the optical end-to-end test of the *Far-Ultraviolet Spectroscopic Explorer* (FUSE)," *Proc. SPIE* **3765**, pp. 470—481, 1999.
14. J. F. Osantowski, R. A. M. Keski-Kuha, H. Herzig, A. R. Toft, J. S. Gum, and C. M. Fleetwood. "Optical coating technology for the EUV," *Adv. Space Res.* **11**, pp. 185—201, 1991.
15. R. A. M. Keski-Kuha, J. I. Larruquert, J. S. Gum, and C. M. Fleetwood. "Optical coatings and materials for ultraviolet space astronomy," in *Ultraviolet-Optical Space Astronomy Beyond HST*, J. A. Morse, J. M. Shull, and A. L. Kinney, eds., APS Conference Series **164**, pp. 406—419, 1999.
16. C. M. Oliveira, K. Retherford, S. J. Conard, R. H. Barkhouser and S. D. Friedman. "Aging studies of LiF coated optics for use in the far ultraviolet," *Proc. SPIE* **3765**, pp. 52—60, 1999.

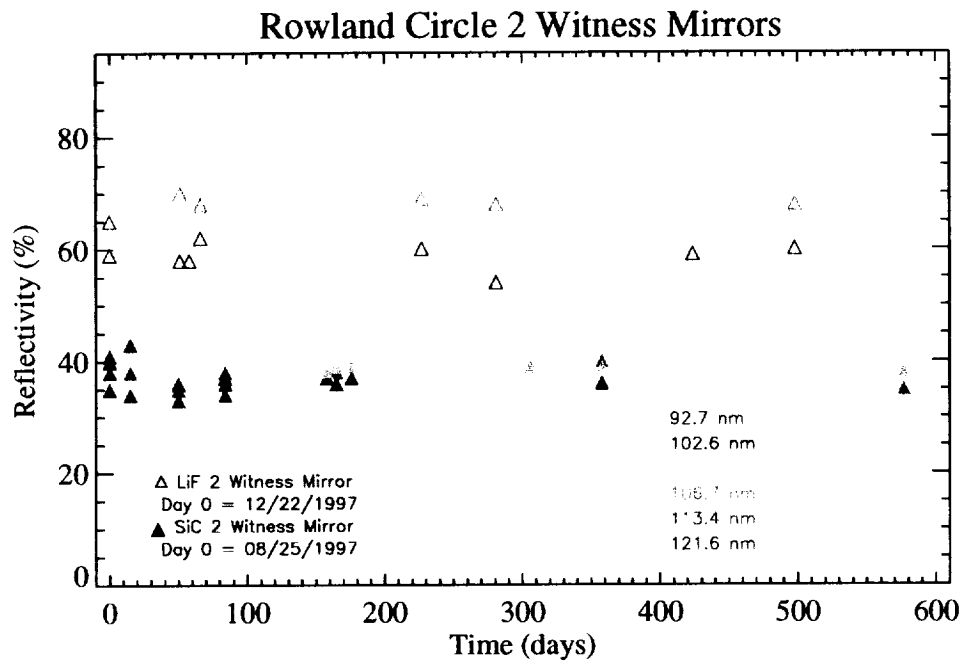
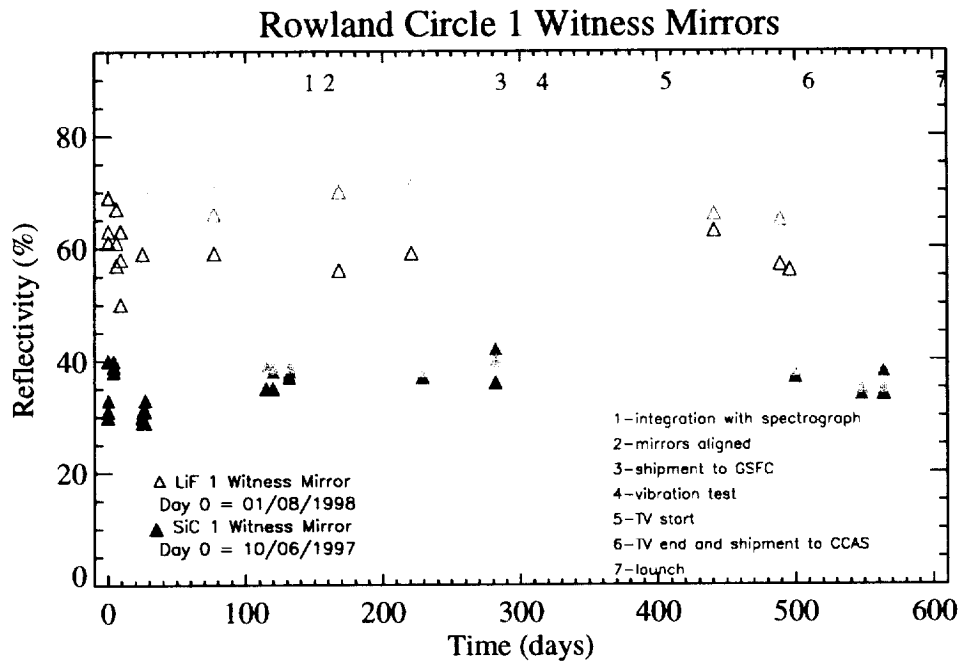


Figure 6. Flight mirror FUV reflectivity as a function of time during *FUSE* satellite integration and test.